EUROPEAN ORGANIZATION FOR NUCLEAR RESEARCH

PSCC/81-45
PSCC/M89
PS/DL/LEAR Note 81-4
$\bar{p}$p LEAR Note 95
KfK-Primärbericht
11.01.02.P10C
1 September 1981

IMPLICATIONS OF AN INTERNAL TARGET FOR ANTINEUTRON PRODUCTION IN LEAR

M. Giesch, J. Gspann, W. Hardt, K. Kilian, P. Lefèvre,
D. Möhl (editor), H. Poth, P. Riboni

ABSTRACT

Starting from the required characteristics of an internal gas target for antineutron production, we discuss the implications for the machine. The admissible target thickness in the presence of the beam cooling-system is worked out and the resulting vacuum requirements are evaluated. The compatibility of the basic machine design with the later installation of the target is examined.

* * *

CONTENTS

		Page
1.	INTRODUCTION	1
2.	CHARACTERISTICS OF AN OPTIMIZED TARGET	1
	2.1 Internal target thickness	1
	2.2 Antineutron rates	3
3.	PRESENT AND FUTURE IMPLICATIONS FOR THE MACHINE	4
	3.1 Generalities	4
	3.2 Target locations	5
	3.3 Implications for the magnet design	6
	3.4 Implications for the vacuum chamber	6
	3.5 Vacuum requirements	7
	3.6 Cooling	9
	3.7 Operational sequence	9
	3.8 Diagnostic and control of the machine	10
	3.9 Future improvements	10
REFERENCES		12
APPENDIX		13

1. INTRODUCTION

The installation in LEAR[1] of an internal hydrogen target[2,3] provides the possibility of antineutron production for subsequent $\bar{n}$-experiments[4]. Maximal antineutron rates for a given load on the PS can be obtained. The operation of LEAR with a sufficiently thick internal target can, however, only be performed in the presence of a beam cooling-system strong enough to compensate the beam blow-up due to multiple scattering on the target. In the following section, the different aspects of an optimized target are worked out. In Section 3 the implications for the LEAR design are discussed.

2. CHARACTERISTICS OF AN OPTIMIZED TARGET

2.1 Internal target thickness

A stored beam undergoes Coulomb and strong interactions when it traverses the target. Small-angle scattering sums up with each passage and produces a beam blow-up which leads to unwanted beam losses. This multiple scattering blow-up can be compensated by a cooling system which achieves cooling times smaller than the multiple scattering blow-up time. Then the beam losses are reduced to scatters larger than the machine acceptance or to inelastic reactions. In this case and in the absence of other losses (resonances, residual gas, beam extraction), the stored beam intensity decays as

$$\frac{N}{N_0} = e^{-\sigma L \rho d f t} , \qquad (1)$$

with a time constant

$$\tau = \frac{1}{\sigma \cdot L \cdot \rho d \cdot f} = \frac{2\pi R}{L \cdot \rho d \cdot \beta\sigma \cdot c} ,$$

where

σ = $\Delta\sigma + \sigma_{st}$,

L = Avogadro's number (6×10^{23} molecules/mole),

ρd = target thickness (in g/cm^2),

f = $\beta c/2\pi R$ = revolution frequency,

$2\pi R$ = machine circumference = 78.54 m,

β = v/c of circulating particles.

The total cross-section σ can be decomposed into a cross-section ($\Delta\sigma$) for Rutherford scattering under angles larger than the machine acceptance θ_0 at the position where the scattering occurs,

$$\Delta\sigma = \sigma_{Ruth}(\theta > \theta_0) = \frac{4\pi r_p^2}{(\gamma - 1/\gamma)^2\theta^2} \quad , \tag{2}$$

where

r_p = classical proton radius = 1.5×10^{-16} cm,

$\gamma = (1-\beta^2)^{-\frac{1}{2}}$,

θ_0 = maximum scattering angle acceptable without loss (in rad),

and into the strong interaction cross-section σ_{st}, which can be parametrized as[5]

$$\sigma_{st} = \frac{55.3}{p_{\bar{p}}} + 60.5 \text{ mb} \qquad p_{\bar{p}} \text{ in GeV/c.}$$

Whilst $\beta\sigma_{st}$ varies only little with the antiproton momentum, the Coulomb scattering dominates at low momenta. Since the Rutherford scattering is inversely proportional to the square of the cut-off scattering angle, an increase of the machine acceptance θ_0 at the target position considerably reduces the Coulomb losses at low energies[2]. In Fig. 1 the behaviour of these cross-sections is plotted versus the $\bar{p}$ momentum for acceptance angles of 6 mrad and 15 mrad.

The target thickness has to be chosen in such a way that the beam lifetime is of the order of the refilling period of $\bar{p}$'s into LEAR. This guarantees the optimum duty cycle. For normal operation the refilling period is fixed such that 10^9 $\bar{p}$'s are transferred every 10^3 s. For special operations a longer cycle (say, 10^{10} $\bar{p}$'s filled every 10^4 s) can be contemplated. The optimal target thickness can then be calculated from Eq. (1),

$$\rho d = \frac{2\pi R}{\beta\sigma \cdot L\tau c} \quad , \tag{3}$$

and is plotted in Fig. 2 for acceptance angles of 3 mrad, 6 mrad, and 15 mrad, and for $\tau = 10^3$ s and 10^4 s. It can be seen from the plot that even for 10^3 s the maximal thickness never exceeds 5×10^{-9} g/cm^2, which is reached at high energies irrespective of the acceptance. At low energies, the target density can be one to two orders of magnitude smaller, depending on the acceptance angle. It should be noted that if it is difficult to reach the maximum target thickness, optimum count rates can still be achieved by reducing the target density and increasing the refilling period and the number of $\bar{p}$'s correspondingly.

A given target density ρd corresponds to a ring-averaged pressure of

$$P_{target}(H_2) = \frac{\rho d/2\pi R}{\rho_0} P_0 \frac{\Theta^2}{\Theta_0^2} ,$$

where

$\rho_0 = 9 \times 10^{-5}$ g/cm^3 = H_2 density at normal pressure,

$P_0 = 760$ Torr,

Θ_0 = acceptance angle at the target ($\simeq$ 6 mrad),

Θ = ring-averaged acceptance ($\simeq$ 3 mrad at normal working point).

The factor Θ^2/Θ_0^2 accounts for the variation in scattering acceptance such that a residual gas of pressure P_{target} all around the ring leads to the same loss rate as the localized target. Inserting numbers, we get

$$P_{target}(H_2)\ [\text{Torr}] \simeq 2.5 \times 10^2\ \rho d\ [\text{g/cm}^2] .$$

The nitrogen equivalent pressure is a factor $Z^2(N_2) = 49$ lower. In order to have $\bar{p}$ interactions essentially only in the internal target, the residual gas pressure should be at least a factor of 10 lower than the ring-averaged target pressure:

$$P_{res}(N_2)\ [\text{Torr}] \leq \frac{2.5 \times 10^2}{10 \times 49}\ \rho d\ [\text{g/cm}^2] \simeq \frac{1}{2}\ \rho d\ [\text{g/cm}^2] . \qquad (5)$$

This condition is consistent with the LEAR design vacuum, as will be discussed in Section 3.6.

2.2 Antineutron rates

The number of $\bar{n}$ produced in the charge-exchange (CEX) reaction for a given target thickness ρd and stored $\bar{p}$ intensity $N_{\bar{p}}$ is

$$R_{\bar{n}} = N_{\bar{p}} \cdot L \cdot \sigma_{CEX} \cdot \rho d \cdot f . \qquad (6)$$

The maximal $\bar{n}$ flux is obtained when the stored beam lifetime is only determined by the $\bar{p}$ interaction in the target. Hence inserting Eq. (3) in Eq. (6) we get

$$R_{\bar{n}} = \frac{N_{\bar{p}}}{\tau} \cdot \frac{\sigma_{CEX}}{\sigma} , \qquad (7)$$

where σ_{CEX} is the charge-exchange cross-section. Since $N_{\bar{p}}/\tau$ should be equal to the $\bar{p}$ accumulation rate (10^6 s^{-1}), the $\bar{n}$ rate can only be maximized by optimizing

σ_{CEX}/σ. Whilst at high energies $\sigma_{CEX}/\sigma \approx \sigma_{CEX}/\sigma_{st} \approx 0.06$, the $\bar{n}$ rate at low energies depends strongly on the ratio $\sigma_{CEX}/\Delta\sigma$. The measured charge-exchange cross-section between 300 MeV/c and 900 MeV/c is well fitted by[6]:

$$\sigma_{CEX} = 17.4 \frac{\sqrt{1 - (0.098/p_{\bar{p}})^2}}{1 + 2.0\ p_{\bar{p}}^2 - 0.45\ p_{\bar{p}}} \qquad (p_{\bar{p}} \text{ in GeV/c}) \ .$$

This parametrization is used to calculate σ_{CEX}/σ and, in turn, the total $\bar{n}$ rate in the low-energy region for different acceptance angles under the assumption that no other beam losses contribute significantly, i.e. no extraction or residual gas losses, etc. In order to get a rough estimate of the $\bar{n}$ yields into a given solid angle, we have evaluated the laboratory angular distribution of the $\bar{n}$'s under the assumption of an isotropical c.m. production for a point-like target and a zero emittance beam.

At 430 MeV/c we compared the isotropic production with the experimentally measured production[7] and the resulting laboratory distributions. The effect at this momentum is that with an isotropic production the small-angle forward production is underestimated by a factor of almost 3. We use the assumption of isotropy, however, to derive a conservative estimate for the rate of $\bar{n}$'s produced into a given forward solid angle. This is plotted in Fig. 3 assuming an acceptance angle Θ_0 = 6 mrad for Coulomb scattering at the target.

It can be seen from this figure that at production momenta close to threshold, about 6 $\bar{n}$/min leave the ring through the 100 × 60 mm^2 elliptical opening of the tangential extension tube, at about 1.4 m from the target, corresponding to a solid angle of ≃ 2.3 msr. This flux increases to about 60 $\bar{n}$/s for higher $\bar{p}$ momenta. The $\bar{n}$ rates are higher if also those $\bar{n}$'s that traverse the vacuum chamber directly are taken into account. The corresponding rates for a forward angle of 14 msr are shown in the upper curve of Fig. 3.

3. PRESENT AND FUTURE IMPLICATIONS FOR THE MACHINE

3.1 Generalities

Following upon the idea of installing an internal target for the production of antineutrons in the LEAR magnet[2], a certain number of provisions have been made in order to facilitate this future option[1]. Wherever it was possible without increasing the cost and/or complexity too much, these provisions have been included in the basic design of the machine. More complicated modifications will have to be postponed to a later date when the option will be implemented. Nevertheless, they have been anticipated so as not to "close doors".

Implications of the first type are:

- the organization of the space in and around the LEAR ring,
- the design of the magnet (including its foundations and supports),
- the vacuum chamber in the magnet (including "stubs" for the introduction of the jet and the exit pipe for secondaries),
- the pumping system,
- beam observation and orbit control.

Implications of the second type include many of the points mentioned above and, in addition:

- operational sequence,
- special diagnostic,
- cooling,
- a low beta insertion,
- additional locations for an $\bar{n}$ target.

These points will be discussed in the remainder of the present note, with emphasis on the first-stage provisions.

3.2 Target locations

Three locations, namely straight section SL2 and the centres of the magnet sector BH1 and BH2 (Fig. 4), have been reserved for the later implementation of an internal target[1]. The two magnet locations are well suited for the production of $\bar{n}$ and other neutrals, and will be discussed below mainly because they give access to a secondary beam with a large solid angle around the forward direction.

The secondaries from BH1 emerge into an area where the shielding can be put close to the machine. We therefore propose that the secondaries emerging from BH1 be "piped" into a zone outside the machine enclosure for precision experiments with detectors covering smaller solid angles.

The area around BH2 offers the space to create an "$\bar{n}$ area" inside the shielding enclosure, providing the possibility to install detectors covering large angles close to the machine.

Shielding, magnets, vacuum, and the space around the machine have been designed keeping these future needs in mind.

3.3 Implications for the magnet design

The LEAR magnet (Figs. 5 and 6) was designed to have the yoke on the inside and its opening on the outside of the ring[1]. Although this affects saturation characteristics, as the flux is compressed at the inner arc, this unconventional feature has several advantages for LEAR, e.g. easy exit for the neutrals emerging from the straight sections ($\bar{p}p$ bound states, H^0 from the decay of H^- used for machine tests or formed during electron cooling with test protons). It also simplifies injection and ejection, as the lines can approach straight section 1 under a small angle.

A second design feature is the central gap, which was left free for the introduction of the jet. Each 90° magnet is made of six blocks, as indicated in Figs. 5 and 6. To create a gap it was decided to leave out the wedge-shaped piece between the two central blocks, thus creating an opening of 15° with a width of 24 cm above the orbit. The drop of the bending field along the orbit is given in Fig. 7. Although this might seem to be only a small perturbation, special measures[8] are necessary to re-establish an orbit close to the design trajectory with a constant bending radius in the magnet. The cure adopted is to compensate for the loss of bending in the centre by having a slightly ($\approx$ 4%) higher field in the four central blocks and a slightly lower one in the two outer blocks, as compared to the field giving a constant bending radius. The price is a 4% reduction in the bending capacity (i.e. peak momentum) corresponding (roughly) to the loss of magnetic length due to the gap. More details are to be found in Ref. 8.

The residual magnetic field in the gap along the axis of the jet and the field in the gap region just above and below the magnet are sketched in Figs. 8 and 9. It can be concluded that even for a main field of 17 kG the stray field below the magnet is a few gauss, which is small enough to permit the installation of pumps at this location.

The LEAR magnets will be installed on a concrete foundation below the magnet, as indicated in Fig. 10. To permit installation of pumping equipment under the centre of the sectors BH1 and BH2, the foundations and the supports of the central blocks have been modified for these two sectors as shown in Fig. 10.

3.4 Implications for the vacuum chamber

The vacuum chamber in each of the magnets will be made to follow the curvature of the particle orbit (Figs. 11 and 12). The side walls, onto which the top and bottom plates are welded, are of stainless steel, 8 mm thick. The 6.6 m long chamber for each sector will be mounted in one piece.

Orbit pick-up electrodes will be installed in the chambers, in the second and the fourth block of each 90° magnet. At least five pump manifolds per sector, with a maximum distance of about 2 m, are desirable.

We foresee equipping the chamber in BH1 and that in BH2 with short vertical stubs above and below each chamber, on to which the "chimney" for the entrance and the exit of the jet can later be branched (Fig. 12). A flange with an inner diameter of 100 mm is the maximum that can reasonably be used inside the gap.

In BH1 we foresee another "stub tube" (Fig. 11) through which, later on, neutrals from the target can leave the machine. A tube and a flange with an aperture of 100 × 60 mm^2, similar to the exit tubes foreseen for neutrals emerging from the straight sections, can be installed in a first stage. It will permit the target to be observed under an unobstructed solid angle of about 2.3 msr. The question of installing a "big box" with a much larger horizontal opening has been briefly studied. We propose to postpone such an installation to a later phase as it would add considerably to the complication of the chamber.

As a result of discussions with the users, no $\bar{n}$ exit tube is included in the first-stage design of the chamber in BH2 (Fig. 12). Early $\bar{n}$ experiments here would have to rely on penetration of $\bar{n}$'s through the chamber. This obvious disadvantage has to be balanced against the large horizontal angle (from 0° to almost 90°) accessible without the shadow of the exit tube. However, to permit such a large angle, the first vacuum pump downstream of the target would have to be displaced (this question is under study; the location given in Fig. 11 is preliminary). The resulting pressure bumps would have to be accepted in the target mode.

Again, later on one might install a modified chamber in the target region, for example a device with a thin outer wall. We propose to postpone such a modification to a future stage.

3.5 Vacuum requirements

The LEAR design pressure for normal operation has been specified to give a multiple Coulomb scattering lifetime (emittance blow-up by $\Delta E_{95\%} = 10\pi$ mm·mrad) of $\tau_{ms} \geq 10^3$ s. With an average focusing function $\bar{\beta}_V = 8.5$ m, this requires a ring-averaged pressure (N_2 equivalent for scattering) of[9)]

$$P \lesssim 1.2 \times 10^{-9}\ \beta^2\gamma^2 \qquad \text{(Torr)}\ , \tag{8}$$

where β and γ are the relativistic factors. This condition is most stringent at low momenta because of the strong energy dependence of the Coulomb scattering; it requires, for example, 1.4×10^{-12} Torr at 100 MeV/c.

At higher energies the vacuum requirements can be relaxed for normal operation. This is shown in the second column of Table 1, where the design pressure for various energies is given. The multiple scattering losses considered so far are 20 to 50 times faster than single scattering losses (as was measured in ICE and can also be estimated from theory). The presence of cooling will make it possible to reduce the

multiple to single scattering losses and increase the beam lifetime correspondlingly. However, as it is not clear to what extent cooling and the ultra-slow extraction can coexist, the vacuum has been specified to permit sufficient beam lifetime without cooling.

For efficient internal target operation with the standard filling cycle (10^9 $\bar{p}$ every 10^3 s), a beam residual-gas lifetime of 10^4 s is essential in order to avoid losses in excess of 10% outside the target region (including the halo of the jet). This requires the operation of a cooling system.

The target itself has then to be thick enough to use up the beam in 10^3 s. A target fulfilling this condition is called a "thick target" in the following.

Efficient operation with a thinner target (called "thin target") is possible by filling more $\bar{p}$ at longer intervals (say, 10^{10} every 10^4 s), but in these circumstances the vacuum has to be lower in proportion in order to stay within the 90% target efficiency aim. Note in passing that with the normal filling cycle the thinner target could be used parasitically, i.e. sharing $\bar{p}$ with other experiments, if the operational difficulties can be solved. The desired gas pressure for efficient operation of a thin target is given in column 4 of Table 1.

As a result of the above considerations we conclude that the design pressure [Eq. (8)] is adequate for the operation of a thick target and includes some safety factor. But for a thin target, which may be preferable as it needs less beam cooling and/or gives smaller equilibrium beam size (see Appendix), the high vacuum quality, as it is designed for low energies, is needed also for higher momenta.

Table 1

$\bar{p}$ momentum (GeV/c)	Design pressure [Eq. (8)] (Torr nitrogen equivalent)	Target density ρd for $\tau_{cycle} = 10^4$ s (thin target) (g/cm^2)	Desirable residual gas pressure P_{rest} [Eq. (5)] (Torr nitrogen equivalent)
0.1	1.4×10^{-12}	6.5×10^{-12}	3.3×10^{-12}
0.3	3.7×10^{-11}	1.2×10^{-10}	6.0×10^{-11}
0.6	2.7×10^{-10}	3.8×10^{-10}	1.9×10^{-10}
1.0	9.9×10^{-10}	4.8×10^{-10}	2.4×10^{-10}
2.0	4.4×10^{-9}	5.5×10^{-10}	2.8×10^{-10}

3.6 Cooling

The equilibrium between scattering on the target and cooling is discussed in Appendix. It is shown that the resulting beam emittance is directly proportional to the target thickness and the damping time constant of the cooling system. Figure 13 gives equilibrium emittance and beam size as a function of $\bar{p}$ momentum for different cooling strengths and the two different target thicknesses considered above.

The stochastic cooling system can give damping times of 50 to 100 s at emittance values around 20-40π mm·mrad and for intensities up to, say, 10^{10} p. From Fig. 13 we conclude that the corresponding equilibrium beam size in the presence of the thin target (20 to 40 mm) is acceptable, at least from the point of view of machine aperture.

Electron cooling is expected to achieve damping times of 5 to 10 s [10]. This permits acceptable beam size (20 to 40 mm) at all energies, even for the thick jet. Used in conjunction with the thin target, it permits very well collimated beams of 5 to 15 mm horizontal diameter and high-energy resolution.

3.7 Operational sequence

A typical cycle for dedicated target operation might consist of

- injection,
- stochastic precooling at injection energy,
- transport to the final energy,
- stochastic and/or electron cooling,
- turning on the jet whilst continuing beam cooling,
- turning off the jet and refilling after a suitable time interval.

The thickness of the jet would be chosen to give a multiple scattering consistent with the cooling strength and the desired equilibrium beam size (Appendix). The aim of making best use of the available 10^6 $\bar{p}$/s then fixes the cycle time ($\tau_{cycle} \simeq \tau_{beam}$) and the number of $\bar{p}$ $\left[N_{\bar{p}} = (10^6/s) \cdot \tau_{cycle}\right]$ to be refilled. Note that we assume that the jet can be switched on and off during operation and that the density can be "modulated" within some range.

For parasitic operation ($\bar{p}$ sharing with ejected beams) the target has to be thinner. The compatibility with ultra-slow extraction has to be studied, especially the need to combine strong transverse cooling with the controlled "blow-up" of the momentum spread for extraction on the other side. Possible solutions, e.g. periods of longitudinal heating and extraction with intermittent short periods of cooling

are being investigated. Another inconvenience is that the working point and the acceptance are predetermined by the resonance conditions needed for extraction.

Whilst being hopeful that a satisfactory parasitic mode can be found, we propose to set up the target for dedicated operation for a first series of runs, and to study the implications for extraction and the best working conditions *in situ*. An equivalent target thickness not exceeding the "design pressure" given by Eq. (8) would surely be acceptable. This should still give useful $\bar{n}$ rates at energies above injection.

3.8 Diagnostic and control of the machine

The pick-up electrodes installed around the machine, and especially in the bending magnets concerned, will permit observation of the $\bar{p}$ orbit near the jet region. For the debunched beam the Schottky signals have to be used for this purpose. To steer the beam onto the jet, it would be desirable to have horizontal dipoles a quarter of a betatron wavelength upstream and downstream of the target to create a half-wave bump. Unfortunately, the corresponding locations (almost the centres of the adjacent long straight sections) are not available, so that steering has to be done by combining the existing backleg and dipole windings in a more complicated way. Additional steering can be done by setting the guide field for a slightly "wrong" momentum, thus displacing the beam by $r = \alpha_p(\Delta p/p)$ all around the machine. As the dispersion function is small (α_p = 0.9 m) in the magnet and large (α_p = 3.5 m) in the straight section, this aperture-consuming procedure is limited to, say, ± 5 mm beam displacement at the jet.

Beam intensity and profile monitoring using the normal LEAR diagnostic will be essential during target operation.

To judge the beam-target overlap, it would be desirable to have special secondary particle monitors; these could hopefully be part of the experimental area. Vacuum gauges around the jet are essential for monitoring the vacuum load.

Rapid "switch-over" from the internal target to different operational modes could be achieved by using sector valves to close off the source and the dump part of the jet.

3.9 Future improvements

The beam focusing should be enhanced and thereby the scattering acceptance θ_0 at the target. This could be done by suitable choice of the working point and/or by powering additional quadrupoles. For the magnet target, this possibility needs further study. As special quadrupoles cannot be put close to the target, the same gain (a factor of 10 in scattering acceptance) as in the straight section[11] cannot be expected. The (relatively small) gain that can be obtained by going to a higher working point can be judged from Table 2.

Table 2

Lattice properties and acceptance angle for two working points

Working point	Q_H	2.3	3.2
Working point	Q_V	2.7	2.7
Machine acceptance (phase-space area in π mm•mrad)	A_H	200	130
	A_V	48	42
Properties at target (magnet centre)			
- Acceptance angles (mrad)	θ_H	4.3	6.0
	θ_V	7.3	7.2
	$\theta_0 \simeq \sqrt{\theta_H \theta_V}$	5.4	6.6
- Focusing functions (m)	β_H	10.0	3.5
	β_V	0.9	0.8
	α_p	-0.8	-2.4
- Horizontal beam size for E_H = 20 π mm•mrad (mm)	$\pm a_H$	14	8

REFERENCES

1) G. Plass (editor), Design study of a facility for experiments with low-energy antiprotons (LEAR), CERN/PS/DL 80-7 (1980).

2) K. Kilian and D. Möhl, Gas-jet target in LEAR, CERN $p\bar{p}$ LEAR Note 44 (1979); Antineutron production with an internal target in the LEAR magnet, PS/DL/LEAR Note 81-1, $\bar{p}p$ LEAR Note 90 (1981).

3) J. Gspann and H. Poth, Internal cluster beam target for antineutron production in LEAR, CERN PSCC/81-27 (1981) and KfK report 3198 (1981).

4) C. Voci, Antineutrons at LEAR, *in* Proc. of the Joint CERN-KfK Workshop on Physics with Cooled Low-Energy Antiprotons, Karlsruhe (1979) (KfK report 2836, Editor H. Poth).
H. Poth, $\bar{n}$ beams from external targets, CERN $\bar{p}p$ LEAR Notes 15 and 52 (1979).

5) W. Grein, Nucl. Phys. B121, 255 (1977).

6) R.P. Hamilton et al., Phys. Rev. Lett. 44, 1179 (1980).

7) R. Bizzarri et al., Nuovo Cimento 54A, 456 (1968).

8) W. Hardt and J. Jäger, Choice of reference orbit inside the LEAR magnet, PS/DL/LEAR/Note 81-3, $\bar{p}p$ LEAR Note 93 (1981).

9) W. Hardt, A few simple expressions to check vacuum requirements, CERN-ISR/300/GS/68-11 (1968).

10) H. Haseroth et al., On the use of the ICE gun for electron cooling in LEAR, PS/DL/LEAR/Note 80-7, $\bar{p}p$ LEAR Note 85 (1980).

11) J. Jäger, A low beta insertion for LEAR, PS/DL/LEAR Note 80-1, CERN/$\bar{p}p$ LEAR Note 89 (1980).

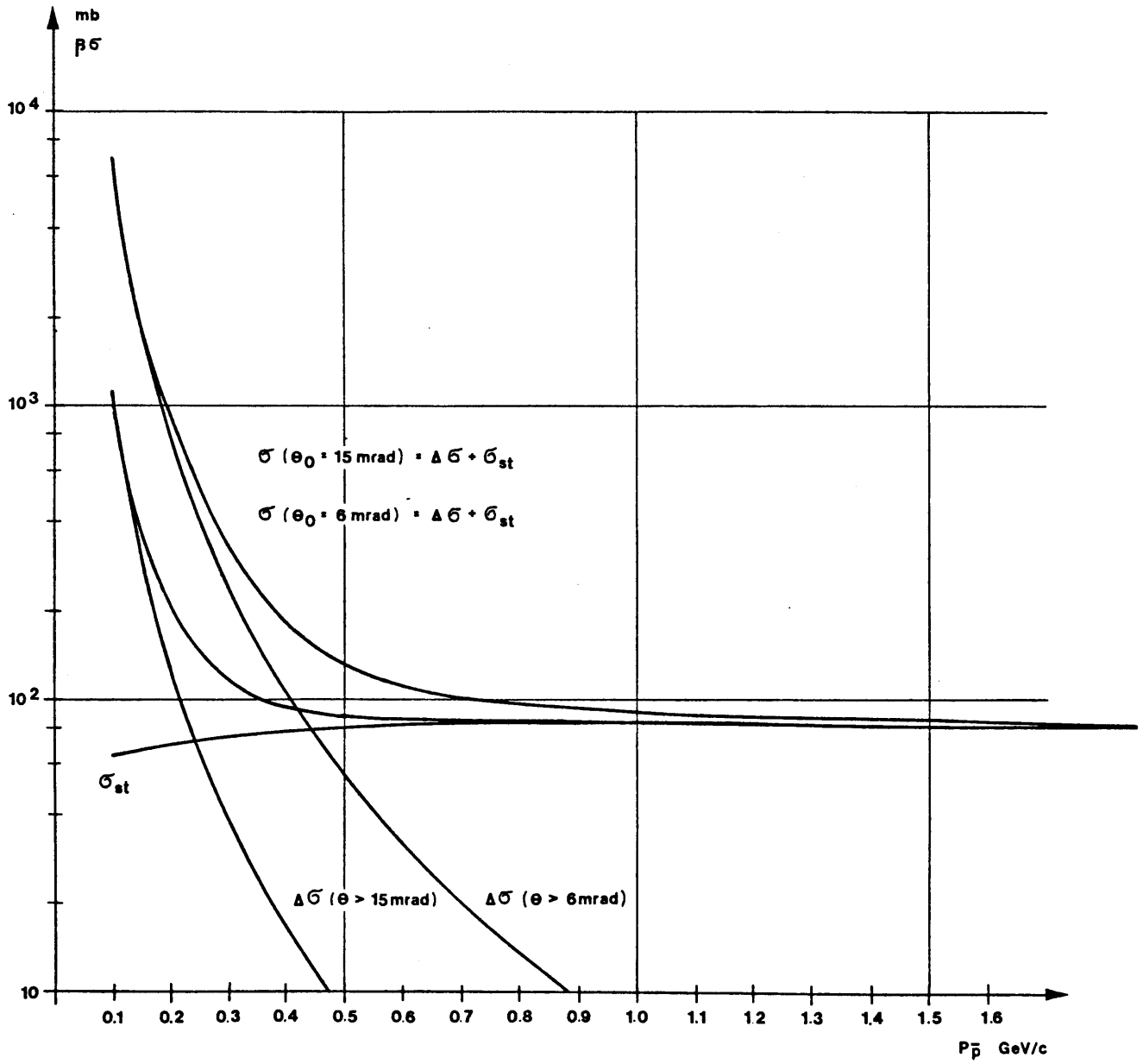

Fig. 1 Coulomb ($\Delta\sigma$) and strong interaction cross-section (σ_{st})

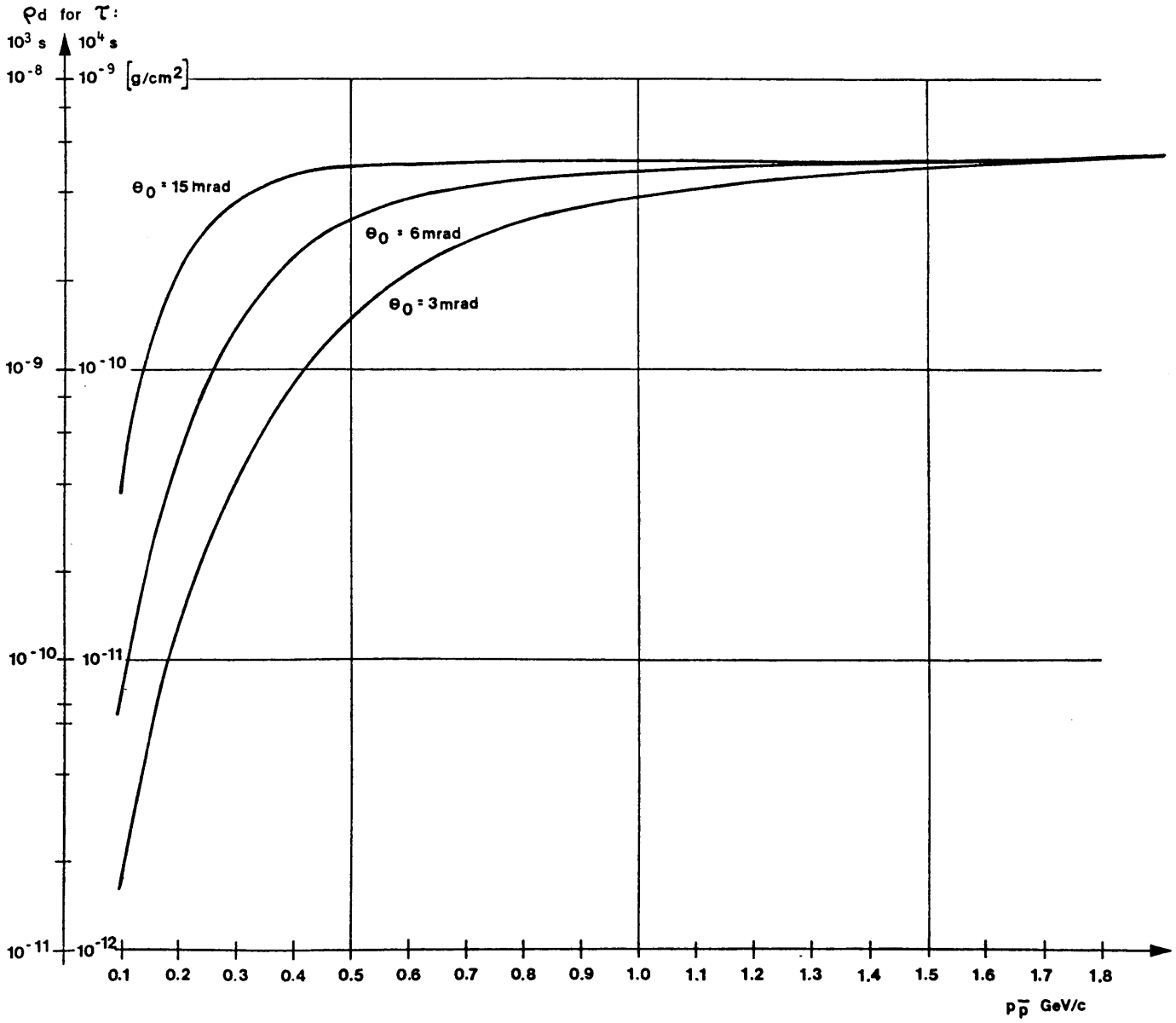

Fig. 2 Maximum target thickness for beam lifetime of 10^3 s (left ordinate scale) and 10^4 s

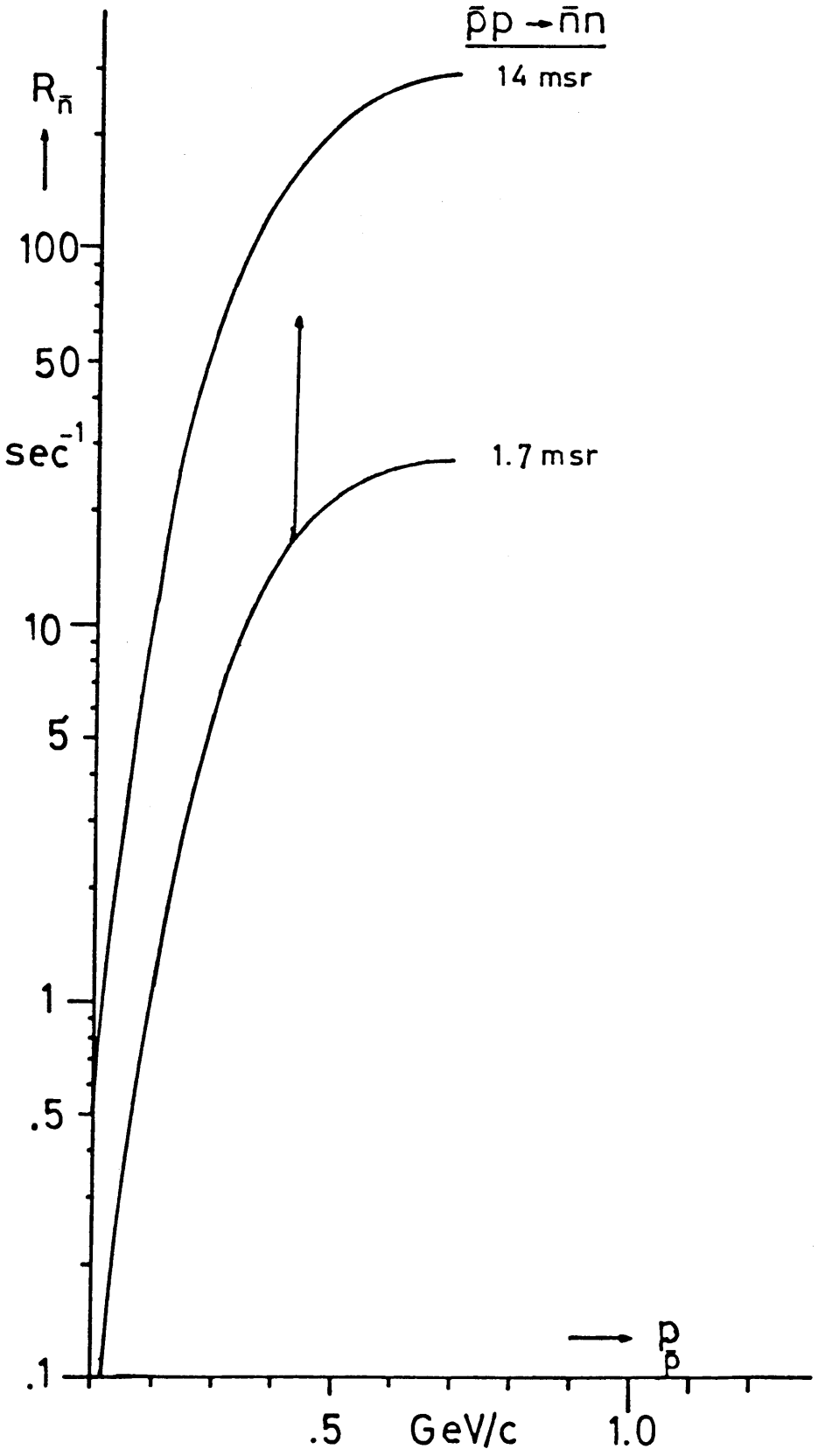

Fig. 3 Number of antineutrons produced into forward angle of 14 and 1.7 msr. (The arrow indicates increase at 430 MeV/c if the assumed isotropical CM-production is replaced by the measured distribution. To calculate Coulomb losses an acceptance angle of 6 mrad is assumed at the target.)

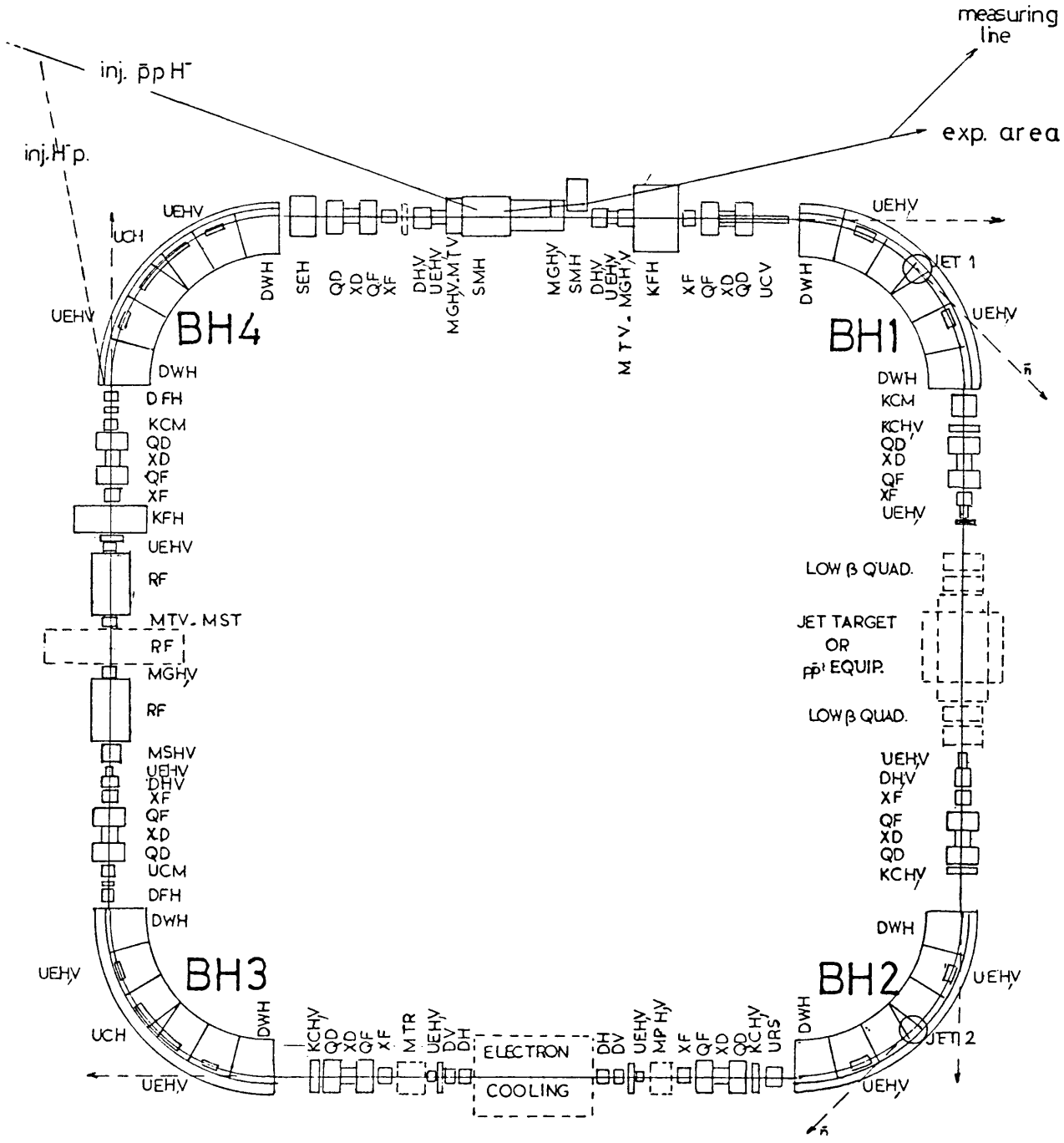

Fig. 4 LEAR: General layout

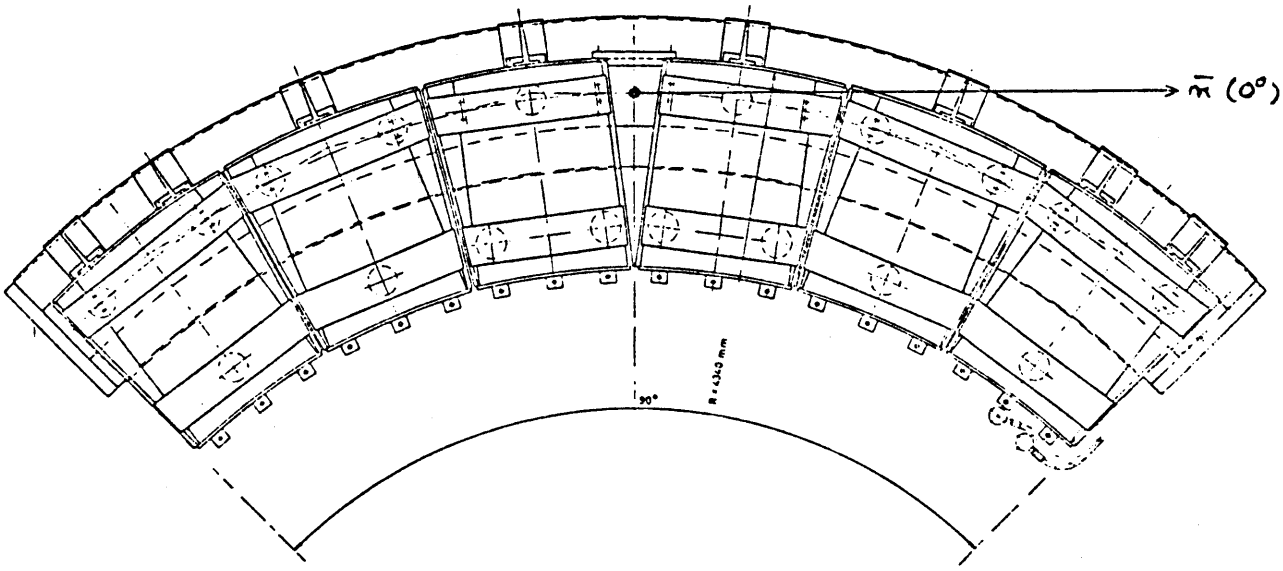

Fig. 5 LEAR bending magnet
top view

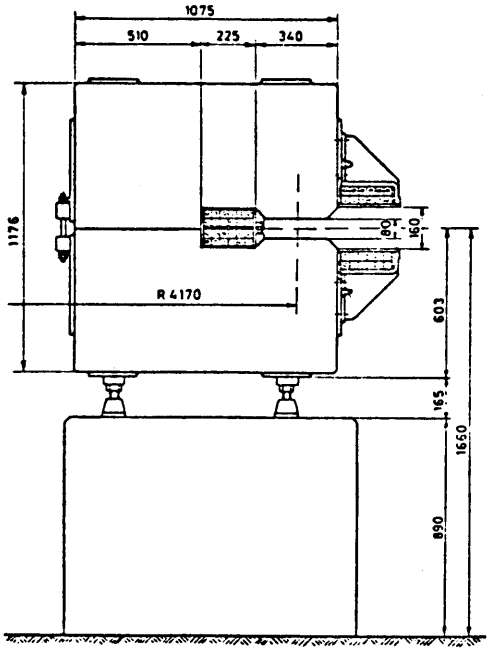

Fig. 6 LEAR bending magnet
front view

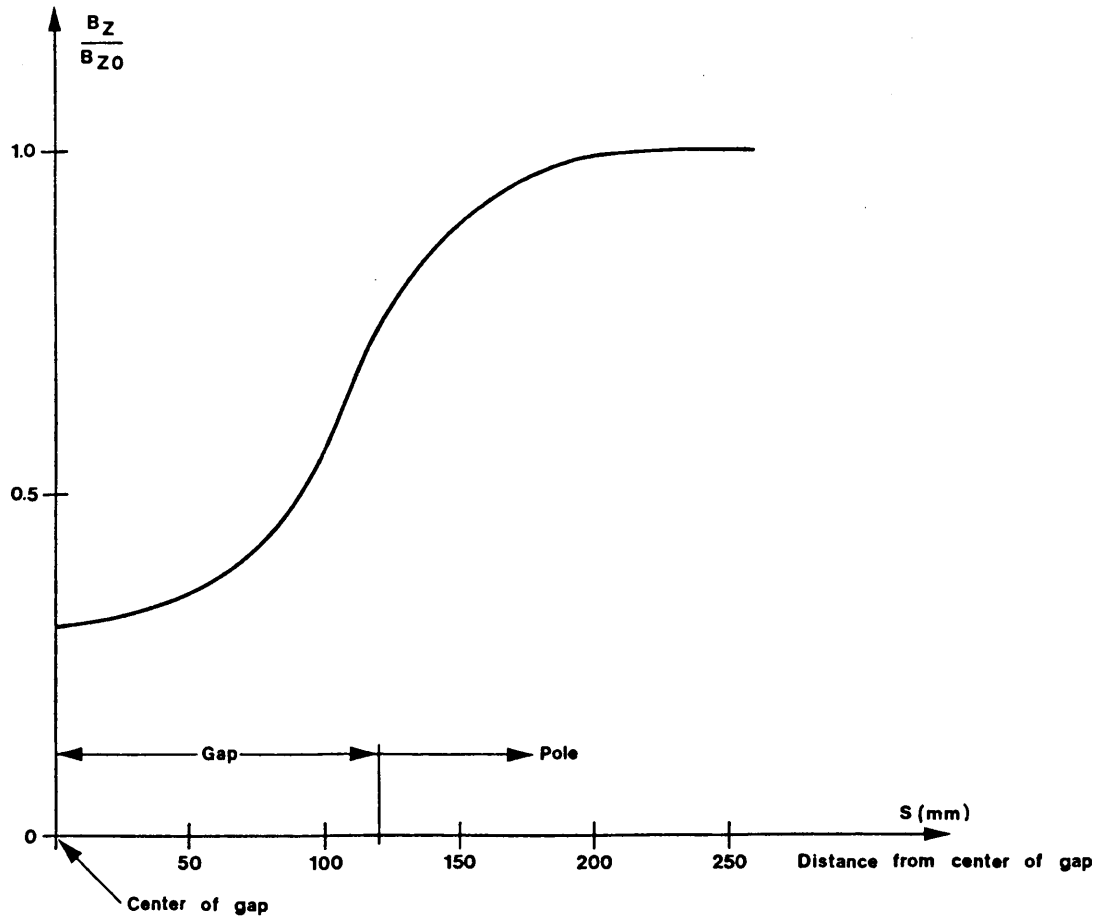

Fig. 7 Bending field at orbit in central magnet

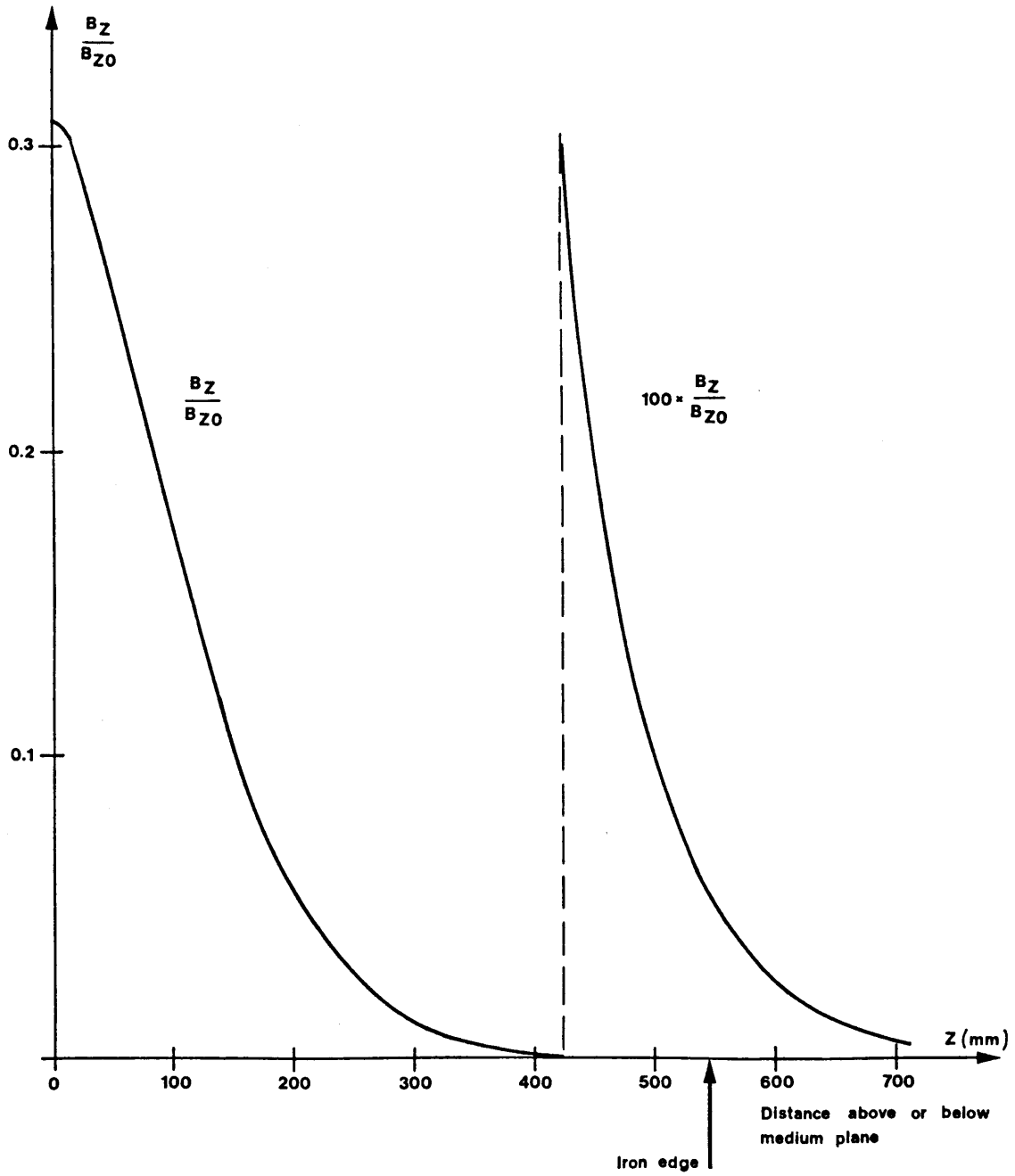

Fig. 8 Stray field along jet axis

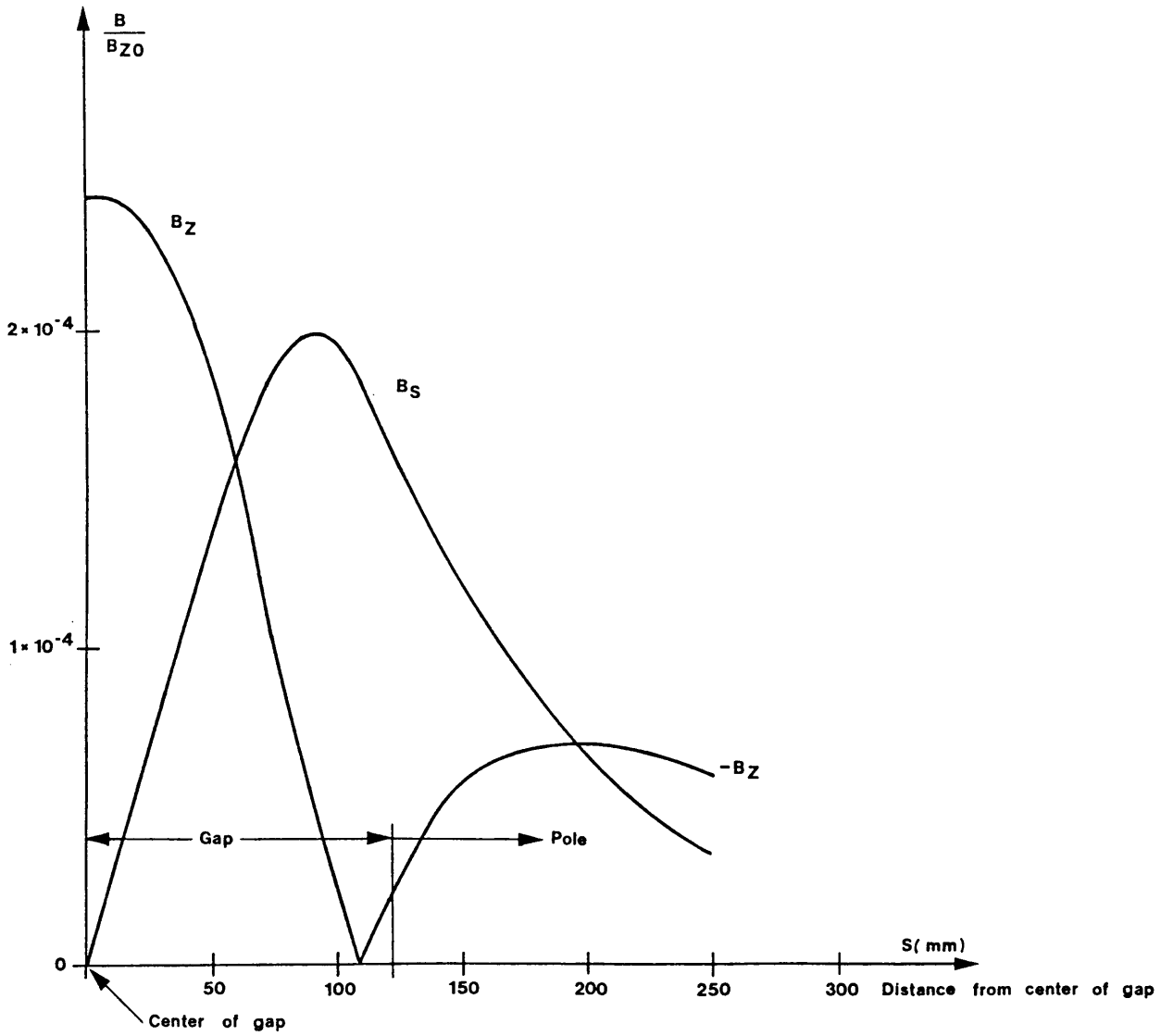

Fig. 9 Stray field just above or below magnet (i.e. at z = 600 mm above the particle orbit)

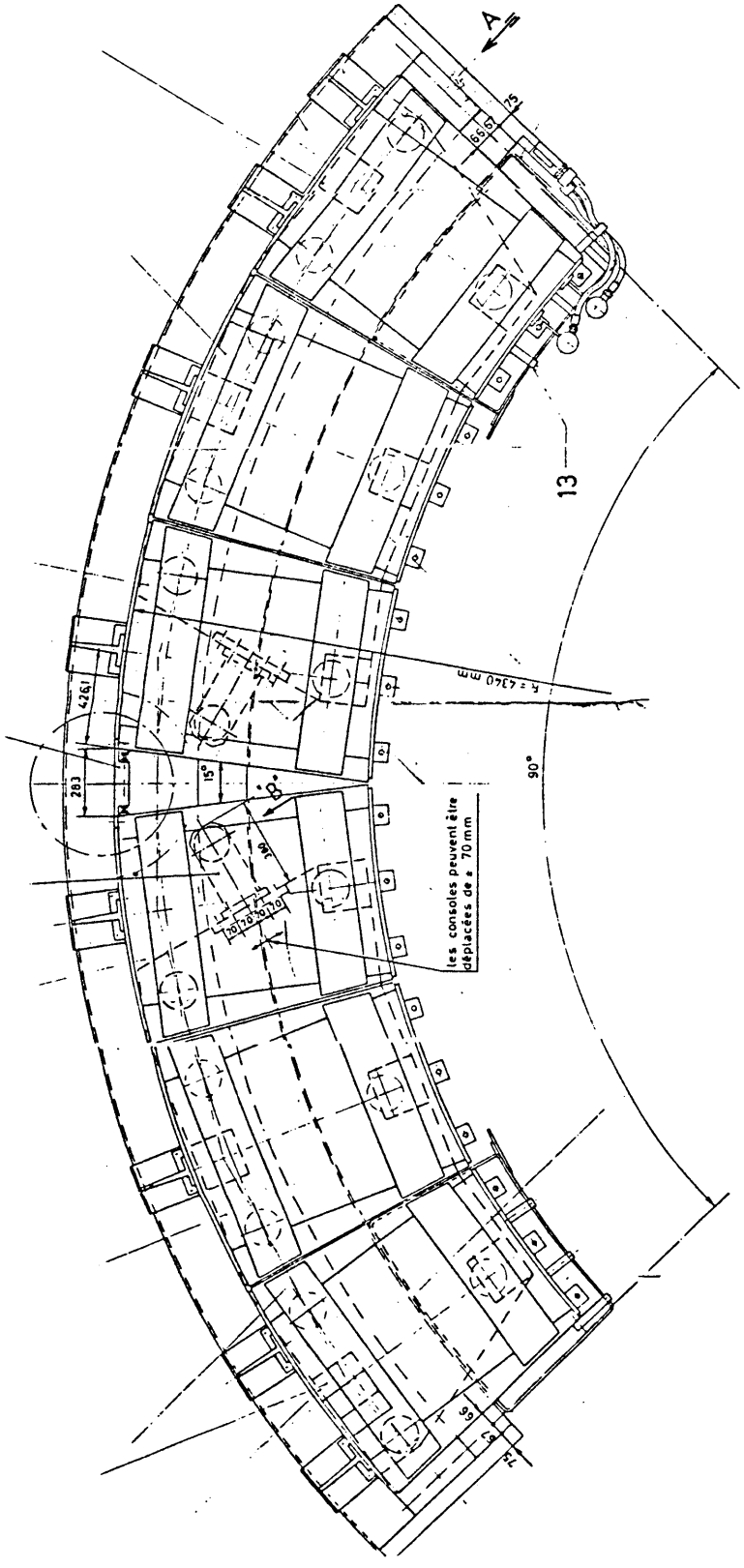

Fig. 10 Modification of magnet foundation in BH1 and BH2

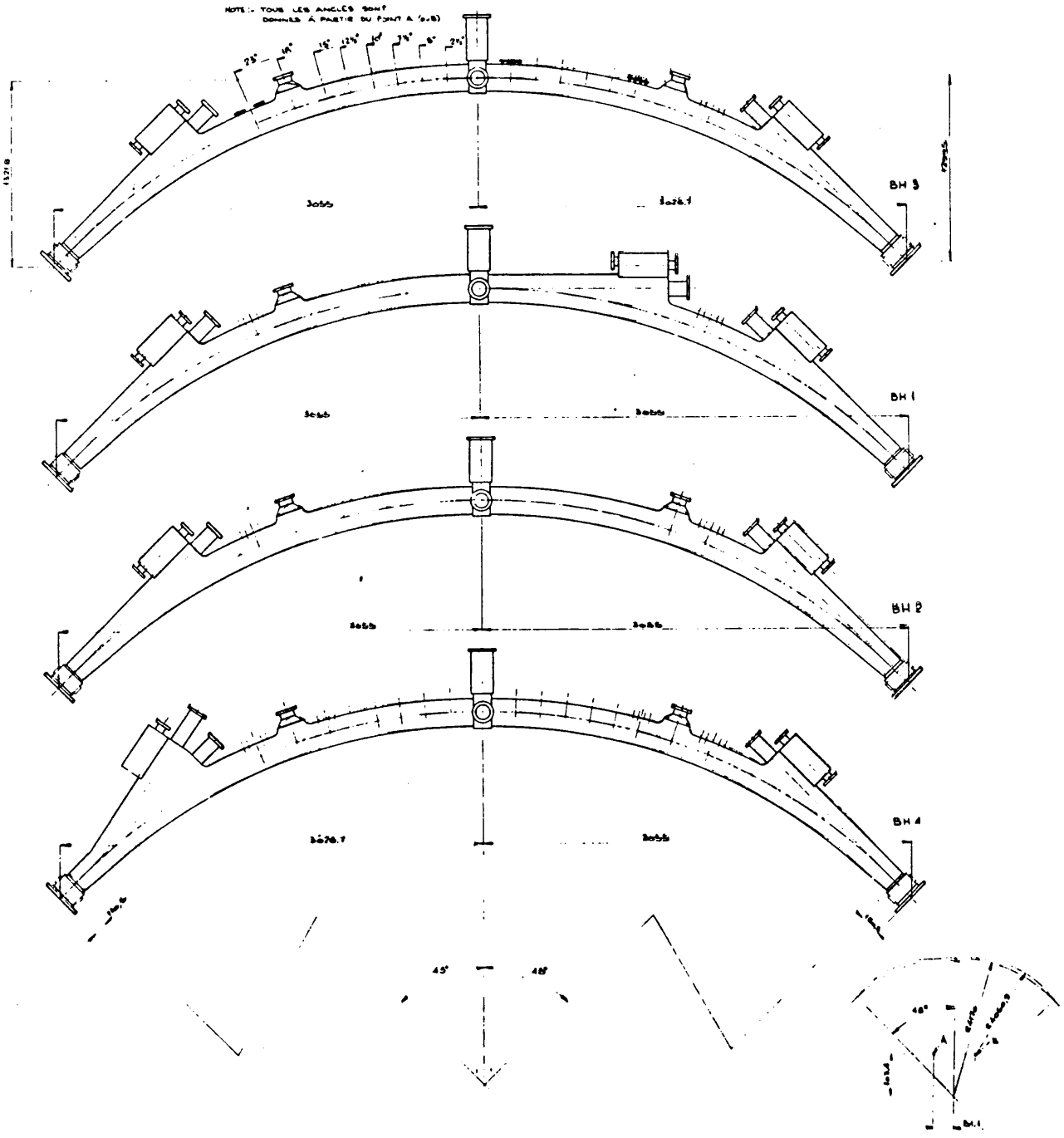

Fig. 11 Vacuum chamber in bending magnets

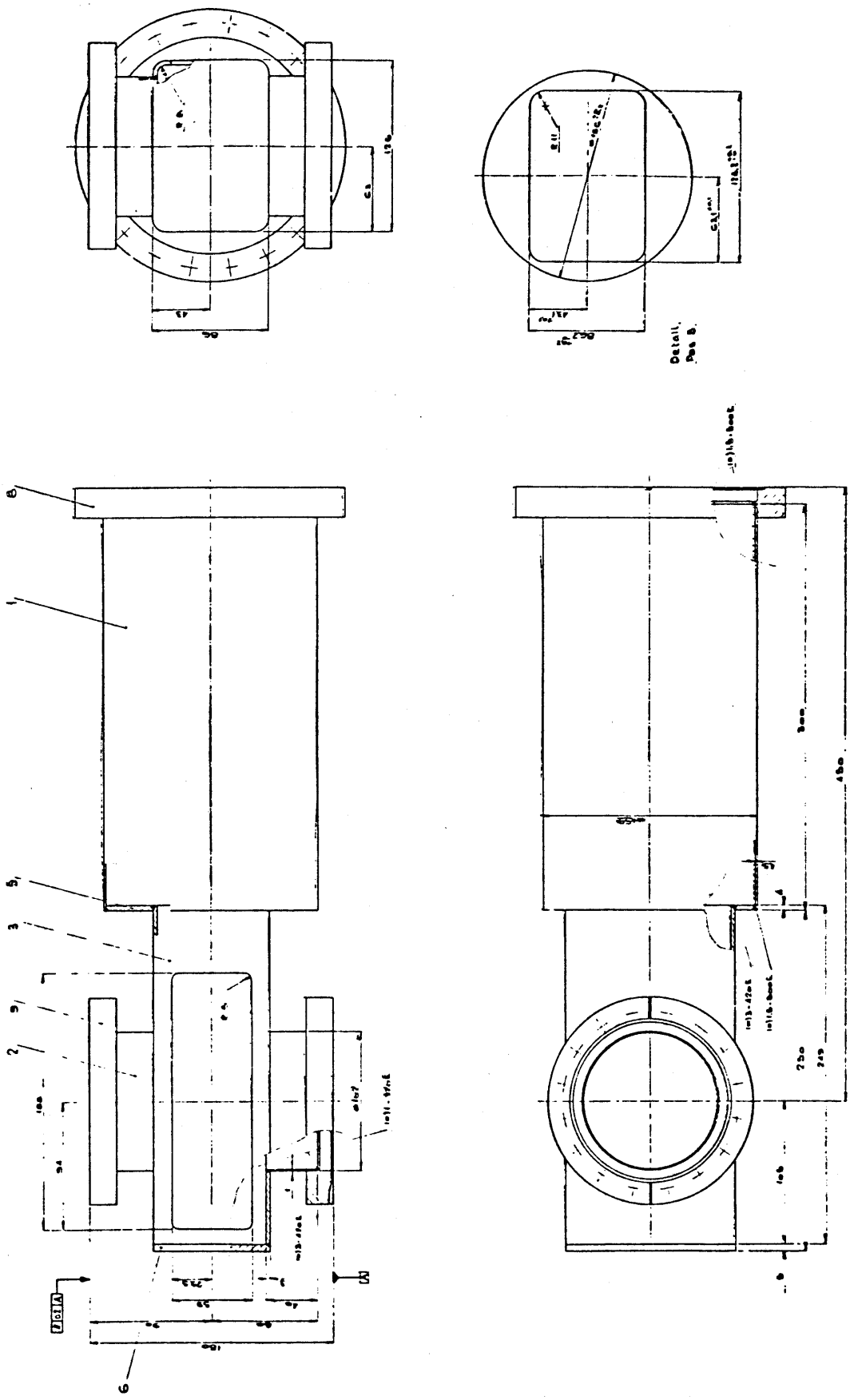

Fig. 12 Central part of vacuum chamber in magnets with flange for entrance and exit of gas jet

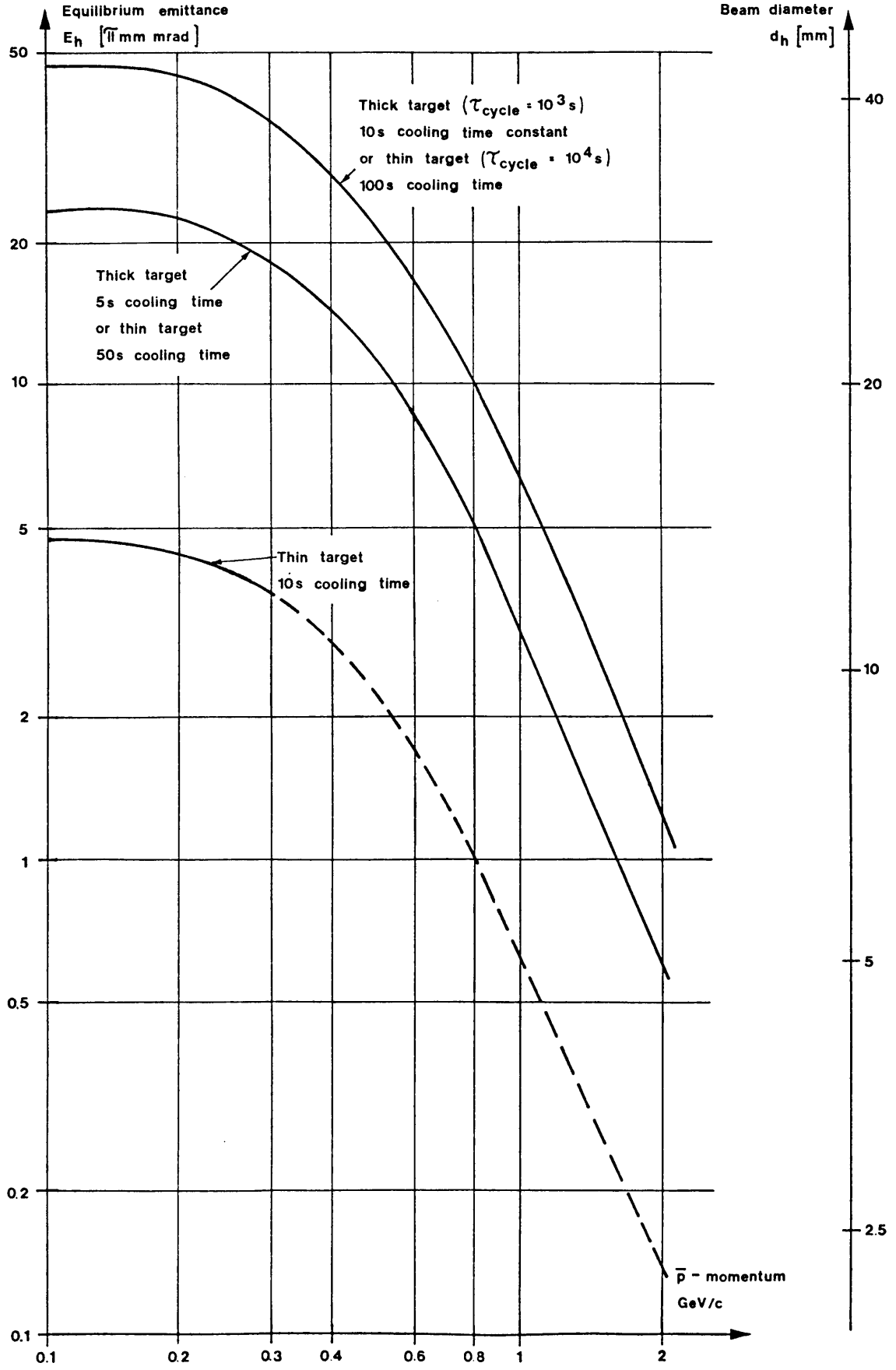

Fig. 13 Equilibrium beam size (horizontal)

APPENDIX

MULTIPLE SCATTERING BLOW-UP VERSUS BEAM COOLING

Multiple scattering on the target (and on the residual gas) leads to a beam blow-up. The increase of the emittance is given by Hardt's formula[9]:

$$\left(\frac{dE}{dt}\right)_{ms} = \dot{E}_{ms} = \frac{0.32\lambda P}{\beta^3\gamma^2}\,|\ln(1-\eta)| \qquad [\pi\ \text{m}\cdot\text{rad/s}]\ ,$$

where η is the fraction of particles contained in the emittance [we use here $\eta = 0.95$, $|\ln(1-\eta)| = 3$], P is the gas pressure in N_2 equivalent, and λ is the ring-averaged β function. For the blow-up on the target the β values at the target position have to be taken ($\beta_H = 10$ m, $\beta_V = 0.9$ m for the usual working point). Expressing the N_2 equivalent target pressure through the target density, we can write for the beam emittance growth rate

$$\dot{E}_{ms} = 19.2\ \beta_{H,V}\ \frac{\rho d}{\beta^3\gamma^2} \qquad [\pi\ \text{m}\cdot\text{rad/s}]\ . \tag{A.1}$$

This growth rate is calculated (Table A.1) for various $\bar{p}$ momenta assuming the nominal target density [Eq. (5)].

Table A.1

$\bar{p}$ momentum (GeV/c)	Target density ρd (g/cm^2)	Emittance growth rate due to multiple scattering: Horizontal $\dot{E}^H_{ms}$ (π mm·mrad/s)	Emittance growth rate due to multiple scattering: Vertical $\dot{E}^V_{ms}$ (π mm·mrad/s)	Energy loss per sec (keV/s)	Equilibrium emittance E^H_{eq} for $\tau_{cooling} = 10$ s (π mm·mrad)
0.1	6.5×10^{-11}	9.8	1.04	4.8	49
0.15	$2\ \times10^{-10}$	9.0	0.95	12	45
0.2	4.7×10^{-10}	9.0 (3.8)	0.95 (0.41)	21	45 (19)
0.3	1.2×10^{-9}	7.0 (1.2)	0.74 (0.12)	41	35 (6)
0.6	3.8×10^{-9}	3.1 (0.16)	0.33 (0.02)	82	16 (0.9)
1.0	4.8×10^{-9}	1.1 (0.04)	0.11 (4.6×10^{-3})	82	5.5 (0.2)
2.0	5.5×10^{-9}	0.24 (8.7×10^{-3})	0.03 ($9\ \times10^{-4}$)	85	1.2 (0.04)

The growth rates given in brackets correspond to a fixed target density of 2×10^{-10} g/cm^2.

The cooling reduces the beam emittance according to

$$\left(\frac{dE}{dt}\right)_c = \dot{E}_c = -\frac{2}{\tau} E \ ,$$

where τ is the amplitude cooling time. Hence the differential equation for the emittance in the presence of multiple scattering blow-up and cooling is

$$\frac{dE}{dt} = \dot{E}_{ms} + \dot{E}_c = \dot{E}_{ms} - \frac{2}{\tau} E \ . \tag{A.2}$$

The integration (for the case where τ is independent of E) yields

$$E(t) = \left[1 - e^{-(2t/\tau)}\right] \frac{\tau \dot{E}_{ms}}{2} + E_0 \, e^{-(2t/\tau)} \ , \tag{A.3}$$

where E_0 is the initial emittance.

The equilibrium beam emittance, virtually reached for $t > {}^3\!/_2\tau$, is

$$E_{eq} = \frac{\tau}{2} \dot{E}_{ms} \ , \tag{A.4}$$

with $\dot{E}_{ms}$ given by Eq. (A.1) and $\tau = \tau(E_{eq})$ in the general case.

Hence we can calculate the required cooling strength for a given target density and an acceptable equilibrium emittance.

The horizontal equilibrium emittance (A.4) is also included in Table A.1 assuming a cooling time constant $\tau_H = 10$ s. Finally Table A.1 gives -- in the last-but-one column -- the average energy loss of a particle in the target. This loss is completely negligible as it can be compensated by an RF system or cooling system supplying an energy gain of a fraction of a GeV per turn.